JOURNAL OF MATERIALS SCIENCE **39** (2004) 4521–4531

TEM and EBSD investigation of continuous and discontinuous precipitation of CrN in nitrided pure Fe-Cr alloys

M. SENNOUR, P. H. JOUNEAU, C. ESNOUF*
GEMPPM, UMR CNRS 5510, Bât. B. Pascal, INSA de Lyon, F-69621 Villeurbanne Cedex
E-mail: claude.esnouf@insa-lyon.fr

Pure Fe-Cr alloys (1 and 3 wt% Cr) were gas nitrided (NH_3, N_2, N_2O mixture at 823 K). Two modes of CrN precipitation: *continuous* (fine disc-shaped precipitates) and *discontinuous* (lamellae-like precipitates) were identified and investigated using transmission electron microscopy (TEM) and scanning electron microscopy (SEM). Both types of precipitates presented a cubic NaCl-type structure and Baker-Nutting orientation relationship with respect to the ferritic matrix. A quantification procedure based on TEM images exploitation revealed that the size and the number of the fine precipitates vary inversely with nitriding depth. This result was compared to the profile of micro-hardness. SEM observations showed that only superficial regions in the Fe-3 wt% Cr were transformed by the discontinuous precipitation of CrN. Electron back-scattered diffraction (EBSD) studies of lamella revealed singular initiation and growth features. A qualitative mechanism of lamella initiation and growth is discussed.

1. Introduction

Nitriding is a surface thermochemical treatment which is often applied to iron-based alloys with the aim to improve their mechanical properties: resistance to mechanical fatigue, wear and corrosion. In the case of chromium steels destined to rolling applications, the required property is the fatigue resistance [1, 2]. That is achieved by the formation of the so-called diffusion zone where the diffused nitrogen atoms are recombined with alloying element(s), especially chromium, to form a fine coherent precipitation which is responsible for a significant hardening and for compression residual strains in the nitrided layer [3].

In addition to the fine coherent precipitation of CrN with platelet-like morphology arranged on a cubic lattice [4, 5], literature reports the occurrence of a lamellae-like precipitation called also *discontinuous* or cellular precipitation [5–7] which is similar to the typical discontinuous precipitation reaction observed in substitutional binary alloys [8].

Discontinuous precipitation involving chromium and nitrogen was extensively studied in high-nitrogen Fe-Cr austenite were the growing lamellas are of Cr_2N [9–13]. However, only few studies have been devoted to CrN discontinuous precipitation occurring principally in nitrided Fe-Cr alloys.

Mortimer *et al.* [5] were the first to observe this type of precipitation when studying a Fe-9.9 wt% Cr alloy. Lamellas were identified by electron diffraction as being of incoherent CrN. Authors spoke then about fibrous precipitation which invade all the matrix and which is responsible of the fall of hardness in the transformed zones.

A similar result was obtained later by Hekker *et al.* [6] and Van Wiggen *et al.* [7], by studying two nitrided (10 vol% NH_3/90 vol% H_2 gas mixture at 833 K) alloys: Fe-3.61 wt% Cr and Fe-3.16 wt% Cr-0.20 wt% C, respectively. However, authors observed that discontinuous precipitation cells start to develop at later stage of submicroscopic precipitation of CrN and they noted the stop of the lamellas growth before all the matrix is transformed.

The present work aims to give progress in the comprehension of initiation and growth mechanisms of CrN precipitation, particularly discontinuous precipitation type, during nitriding using advanced characterization techniques.

2. Experimental procedure

In order to avoid interference with carbon precipitation, pure Fe-Cr alloy (1 and 3 wt% Cr) was supplied by Ecole des Mines de Saint-Etienne (EMSE). Its chemical composition is given in Table I.

Ingots of 10 mm thickness were hot-rolled, cold-rolled and finally rectified in surface in order to obtain a thickness of 1 mm. Before nitriding, specimens were annealed at 923 K during 3 h in silica sealed capsules in order to modulate the grains size and to avoid that a structural transformation like

*Author to whom all correspondence should be addressed.

TABLE I Chemical composition of the two studied Fe-Cr alloys

	Cr	C	S	O	N
Alloy 1	0.95	<0.0010	<0.0010	<0.0010	<0.0010
Alloy 2	2.98	<0.0010	<0.0010	<0.0010	<0.0010

restoration—recrystallization superpose to CrN precipitation. Nitriding was performed at 823 K and at low-pressure (between 200 and 400 mbar) in a gas mixture (NH_3, N_2, N_2O). At this temperature range, only ammonia is dissociated but a recombination of active nitrogen atoms to form molecular nitrogen occurs:

$$2NH_3 \rightarrow 2N + 3H_2 \quad \text{(I.3)}$$

$$2N \rightarrow N_2 \quad \text{(I.4)}$$

To avoid the second reaction, ammonia has been used with N_2O. The reaction between Fe and N_2O leads to the formation of iron oxide (FeO) which in its turn reacts with ammonia to give active atomic nitrogen which diffuse in the material:

$$N_2O + Fe \rightarrow N_2 + FeO \quad \text{(I.5)}$$

$$2NH_3 + FeO \rightarrow 2N + 3H_2O + 3Fe \quad \text{(I.6)}$$

By adding molecular nitrogen in the furnace atmosphere, it is possible to regulate the nitriding rate by dilution, allowing maximum delay of the formation of the combination layer which constitutes a barrier to the nitrogen diffusion.

Scanning Electron Microscopy (SEM) and EBSD observations have been made on the cross-sections of nitrided samples perpendicularly to the nitrogen diffusion direction using a Jeol 840ALGS microscope equipped with an EDX-PGT detector and an EBSD-HKL device. Before observations, the cross-section of nitrided samples was mechanically polished (final stage 1 μm diamond) and then chemically attacked (nital 3%).

TEM investigations were performed on two 200 kV transmission electron microscopes: a Jeol 200CX for conventional imaging and a Jeol 2010F with a field emission gun for high-resolution imaging and nanoanalysis. This latter was equipped with an Energy Dispersive X-ray (EDX) Oxford Instruments device and an EELS Gatan digi-Peels 776 spectrometer. Thin foils were extracted at different depths in the nitrided layer perpendicularly to the nitrogen diffusion direction using prior mechanical abrasion following by chemical electropolishing (46.5% butoxyethanol, 46.5% methanol, 7% perchloric acid) using a Struers-Tenupol 5 apparatus.

3. Results and discussions

3.1. Microstructural aspects of nitrided layers

After a 14 h nitriding at 823 K, chemical contrast SEM images obtained on cross-sections of Fe-Cr specimens (1 and 3 wt% Cr) are shown in Fig. 1a and b, respectively. As it was observed by Kekker *et al.* [6] when studying a nitrided Fe-3.61 wt% alloy, the nitrided Fe-3 wt% Cr alloy exhibits lamellae-like precipitates throughout surface regions. TEM micrographs revealed that lamellas form two orthogonal families which grow without overlap each other (Fig. 2). Their chemical composition was identified by EDX microanalysis as CrN. However, what is interesting is that electron diffraction works reveal that lamellas are arranged according to the Baker-Nutting (ORs) with respect to the iron matrix:

$$(100)_{CrN}//(100)_{Fe}; \quad [110]_{CrN}//[001]_{Fe} \quad (1)$$

During prolonged nitriding, some lamellas globularize and lost their coherency with the ferrite what explains, in part, the low hardness of transformed zones (700 Hv) compared to untranformed ones (1000 Hv).

TEM micrographs obtained on untranformed zones show three orthogonal families of disc-like shape nanometric precipitates (Fig. 3a). As it was mentioned in previous works, diffraction work confirms that precipitates are Baker-Nuting oriented cubic CrN. Streaks in the diffraction pattern correspond to CrN reflections and so indicates the very small thickness of these precipitates which is about a few atomic layers as it clearly showed by the HRTEM image obtained on one of them (Fig. 3b).

On the other hand, comparison between microhardness and nitrogen concentration (EPMA analysis) profiles across the nitrided layer (Fig. 4) leads us to attribute the observed profile of properties to the decrease of nitrogen contents resulting in the decrease of the precipitation density. The following paragraph aims to analyze quantitatively this microstructural evolution using TEM micrographs.

3.2. Microstructure evolution during nitriding

3.2.1. Continuous precipitation

Considering time—nitriding depth equivalence, thin foils were sliced at different depths in the nitrided layer on the base of microhardness profiles. Hence, for a 14 h nitriding time, thin foils were extracted at 100, 300 and 400 μm depths below the surface corresponding to three precipitation stages: stationary, advanced and in the nucleation step, respectively.

For each depth, precipitates were counted from low magnified TEM images and their mean diameter calculated using image processing methods [14]. The mean thickness of precipitates was estimated from HRTEM Fourier-filtered images. HRTEM images were performed along the $\langle 001 \rangle_{Fe}$ zone-axis. On this azimuth, the revealed CrN atomic planes are those of chromium which are 0.207 nm apart (Fig. 3b).

Precipitates number per volume unit (volume density) has been determined taking into account the local thickness of the analyzed area. This was achieved by exploiting Low-Loss (plasmons) EELS spectra using

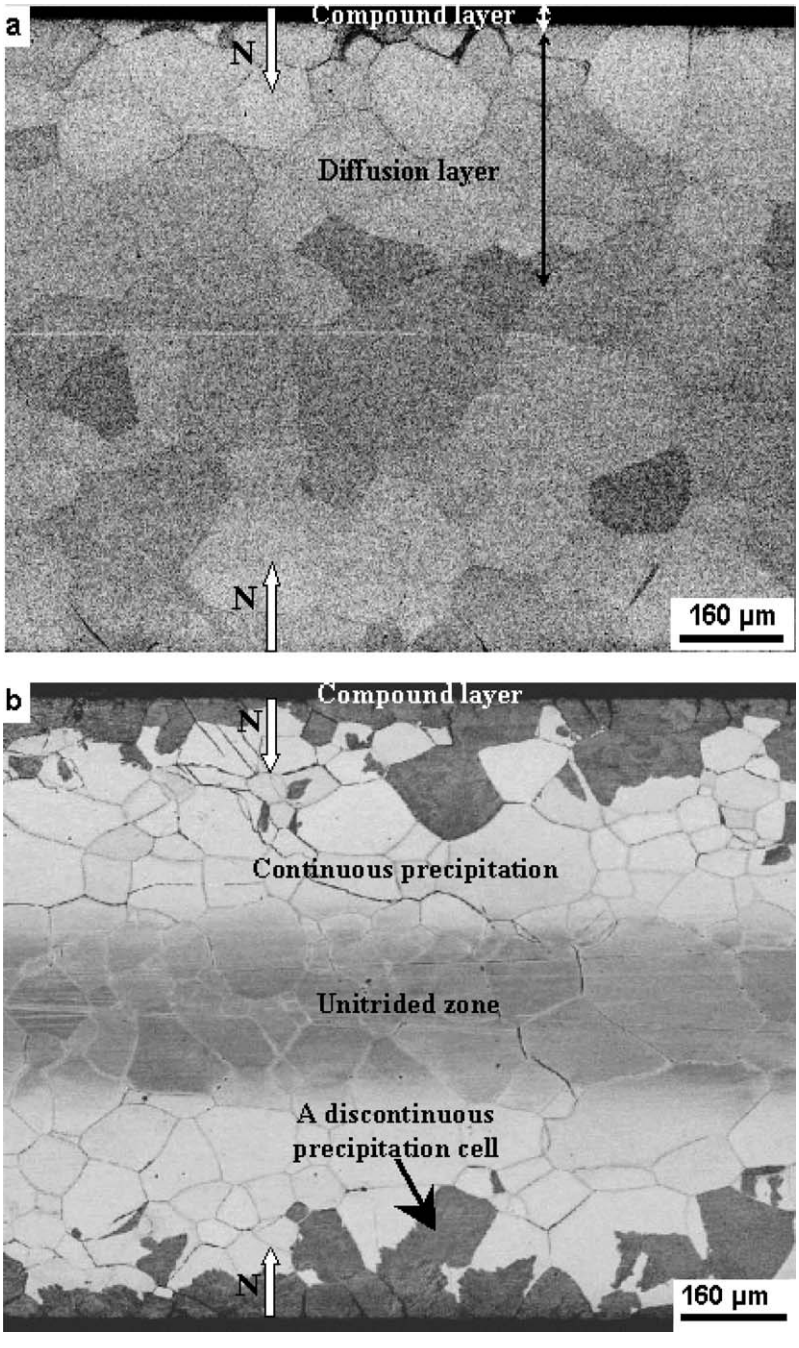

Figure 1 Cross-sectional SEM micrographs obtained perpendicularly to the nitrogen diffusion direction on Fe-Cr alloys nitrided 14 h at 823 K: (a) Fe-1 wt% Cr alloy; (b) Fe-3 wt% Cr alloy. Dark contrast in Fig. (b) indicates regions invaded by CrN discontinuous precipitation.

the well known relation:

$$t = \lambda \ln(I_{ll}/I_0) \tag{2}$$

where λ is the mean inelastic free path of the incident electron going trough the specimen (90 nm for iron at 200 kV accelerating voltage measured using the convergent beam diffraction (CBED) method. I_0 is the intensity under the zero-loss peak and I_{ll} is the intensity of the low-loss portion of the spectrum.

In the case of the Fe-1 wt% Cr alloy, the obtained TEM micrographs show that size (diameter) of CrN precipitates are obviously increasing with the depth while their number is clearly decreased (Fig. 5a and Table II). On the other hand, precipitates thickness measurements deduced from HRTEM images using the Fourier filtering processing do not reveal a significant change through the nitrided layer excepting at 400 μm below the surface where precipitates are less numerous but slightly more thick (remember that an indication of precipitate thickness is given by the streak length

TABLE II Results of microstructural parameters quantification. Mean values are extracted from several hundreds relatively to precipitates diameter. Foil thickness measurements required for volume density determination, were performed using standard method based on low-loss region exploitation in EELS spectra

Material	Fe-1 wt% Cr			Fe-3 wt% Cr		
Depth (μm)	100	300	400	100	300	400
Mean precipitates diameter (nm)	12	16.2	19	5	17	30.5
Density of precipitation (10^5 pp/μm^3)	1.8	1.1	0.34	18	1.6	0.25

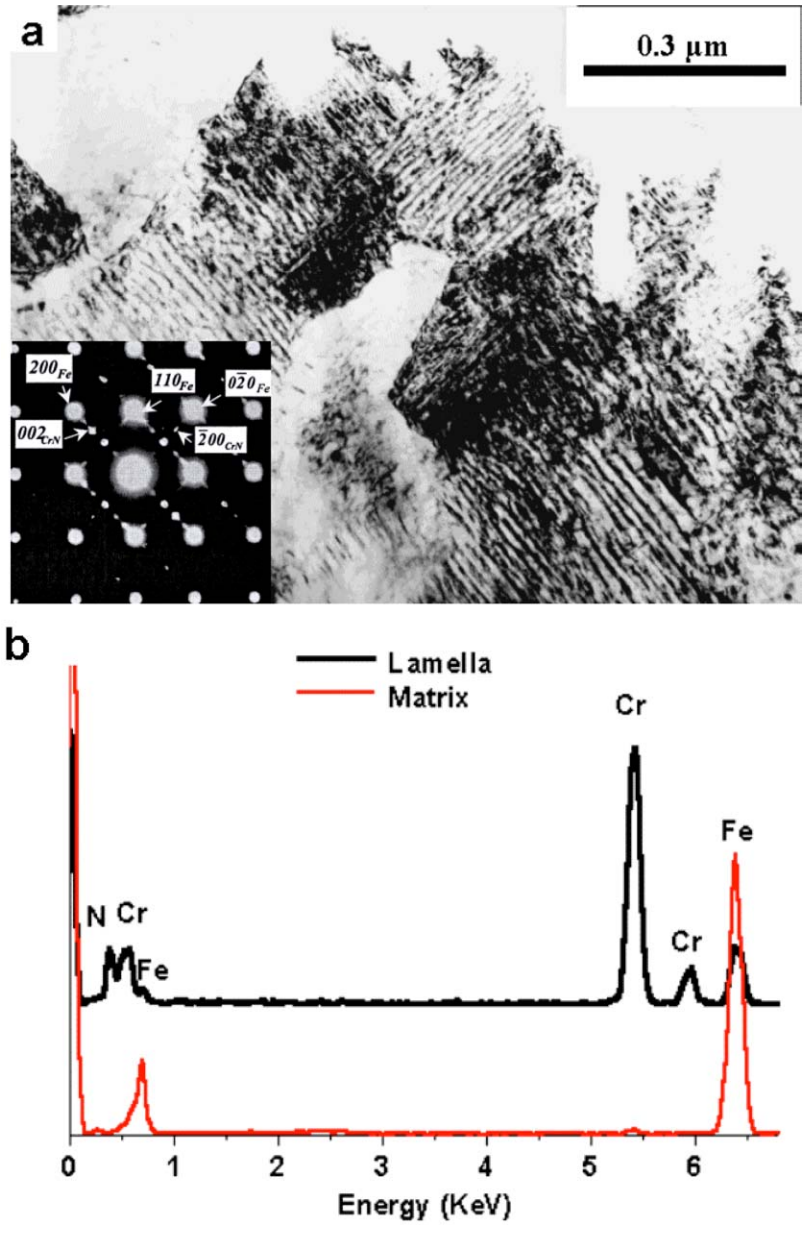

Figure 2 (a) TEM micrograph of discontinuous precipitation cells (Fe-3 wt% Cr alloy). CrN lamellas are arranged into two orthogonal families growing without overlapping. The corresponding selected area diffraction pattern (insert) shows the Baker-Nutting orientation relationship between lamellas and the ferritic matrix. (b) EDX spectra acquired on a CrN lamellae and on the iron matrix between two lamellas.

on diffraction patterns; this latter being the opposite of thickness).

The increasing of CrN precipitates mean diameter with depth is more pronounced in the Fe-3 wt% Cr alloy (Fig. 5b and Table II). Moreover, this is accompanied by a significant precipitates thickening with nitriding time which is attributed to the strong interaction between interstitial and substitutional elements in nitrided high chromium-content alloys [15].

However, it must be noted that this was observed only in the internal untransformed zones (200–400 μm below the surface). Indeed, HRTEM images revealed that continuous precipitation zones located close to the surface, where discontinuous precipitation is predominant, contain a high density of very fine CrN precipitates (1 or 2 atomic layers) which are certainly responsible of the significant measured microhardness ($\sim$1050 Hv). From these features, it was suggested that these precipitates are probably nucleated during the cooling of samples or at the early stage of nitriding before they stop to grow as soon as discontinuous precipitates is initiated. Finally, it can be observed that during all growing process, cubic CrN precipitates preserve the Baker-Nutting (ORs) with the ferrite matrix.

The increase of the precipitates size with the nitriding depth is not expected, since it is in contradiction with the coalescence principle. The correspondence between the time and the depth in the nitrided layer assumes logically that the more depth increases, the more time of contact with nitrogen is short. Therefore, the more depth increases, the more the nitrogen supply diminishes. Nitrides should therefore be smaller when depth increases, but this is not the case.

In order to explain this phenomenon, a qualitative response can be given. In the early stage of nitriding, nitrogen that arrives in the material diffuses rapidly due to the absence of the compound layer, providing thus an important flow of atoms in the surface region. This

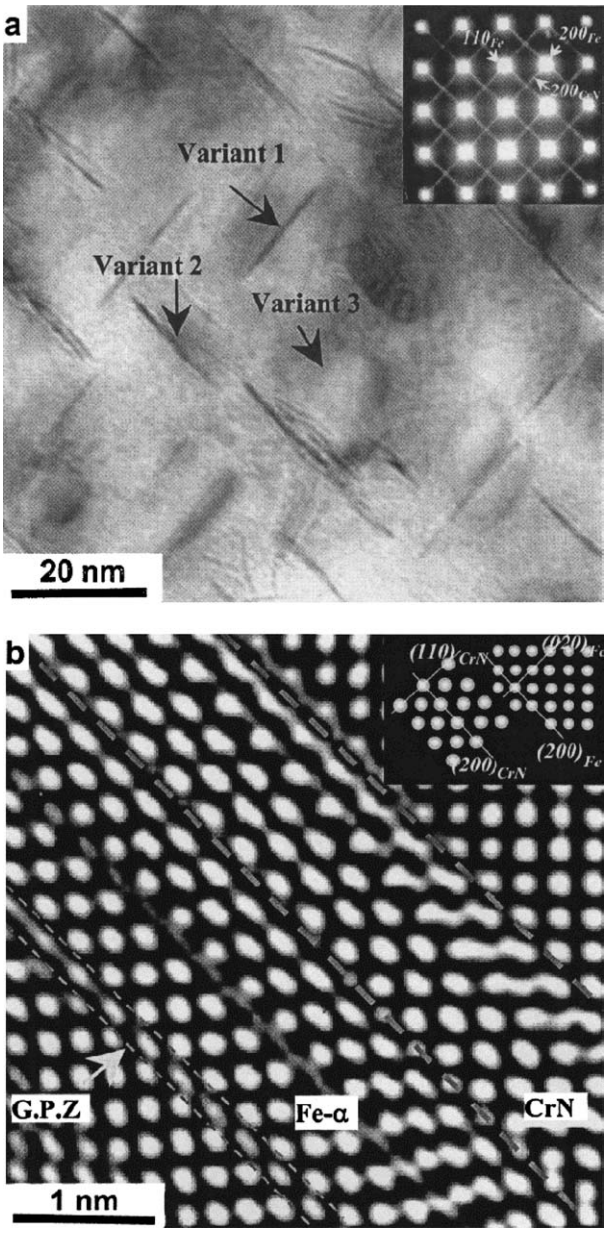

Figure 3 (a) TEM micrograph obtained on a thin foil (Fe-1 wt% Cr alloy nitrided 14 h at 823 K) along $[001]_{Fe}$ zone axis. The corresponding electron diffraction pattern was indexed according to the Baker-Nutting (ORs) between the cubic (NaCl-type) CrN and the cubic (bcc) iron matrix. (b) HRTEM image (after Fourier-filtering) taken on a nanometric CrN precipitate along $[001]_{Fe}$ zone axis allows to appreciate the very small thickness of these precipitates which is about few atomic layers. Planar mono-atomic stacking defect are revealed running parallel to CrN precipitates.

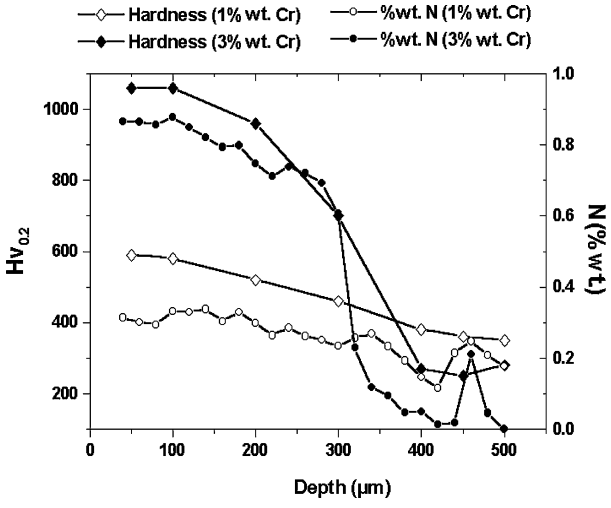

Figure 4 Microhardness (applied load 200g) and nitrogen concentration profiles (EPMA on CAMEBAX-SX apparatus) along cross-sections of 1 and 3 wt % Cr alloys. Microhardness measurements were performed only on grains containing continuous precipitation. Nitrogen concentration peak at around 450 μm from surface in the Fe-3% wt Cr alloy is attributed to a measurement point made on a grain boundary. That reveals the preferential nitrogen diffusion along grain boundaries.

leads to the apparition of a big number of germination sites in this zone. However, the flow of nitrogen decreases progressively with the depth in the nitrided layer (Fig. 4) reducing thus the number of germination sites of CrN nitrides. Consequently, the flow of nitrogen is distributed on a limited number of nucleating precipitates which are therefore on average more bigger than those formed in the superficial zones. These results have an incidence on the mechanical properties evolution inside nitrided layers as consequence of evolution of the fine coherent CrN precipitates. This concerns especially the diminution of the precipitates volume density, thus reducing the number of pinning points for the moving dislocations. In addition, the quantified microstructural parameters were exploited to confirm the Orowan hardening mechanism.

3.2.2. Discontinuous precipitation

Classical discontinuous precipitation is defined as lamellae growth behind a moving grain boundaries. Hence, we suggested that in alloys where such a reaction occurs, a change in the grain size must normally take place. Thus, in order to check if it is the case of the nitrided Fe-Cr alloys, distributions of grain size in an unitrided specimen and in a specimen nitrided during 14 h at 823 K have been investigated. The comparison between the two obtained histograms (Fig. 6) do not show any significant change in grain size which is in contradiction with a boundary migration growth mechanism. Consequently, in order to apprehend the real growth mechanism of the discontinuous precipitation in nitrided Fe-Cr alloys, EBSD technique has been performed.

Fig. 7a and b present a SEM micrograph obtained on a region of discontinuous precipitation in the Fe-3 wt% Cr alloy and the corresponding EBSD map, respectively. On the later, grains having the same crystallographic orientation exhibit the same color.

To study structural and crystallographic dispositions governing the discontinuous precipitation development, we were interested to three zones in the investigated region possibly corresponding to different stages of discontinuous precipitation growth: early stage (zone 1), intermediate stage (zone 2) and final stage (zone 3).

3.2.2.1. Zone 1. For simplification, the grain from which lamellas start growing (*mother grain*), the cell of discontinuous precipitation and the grain in which this later is propagated, are called A_1, B_1 and C_1, respectively. The examination of the corresponding {111} and {110} poles figures (Fig. 8a) allows to observe

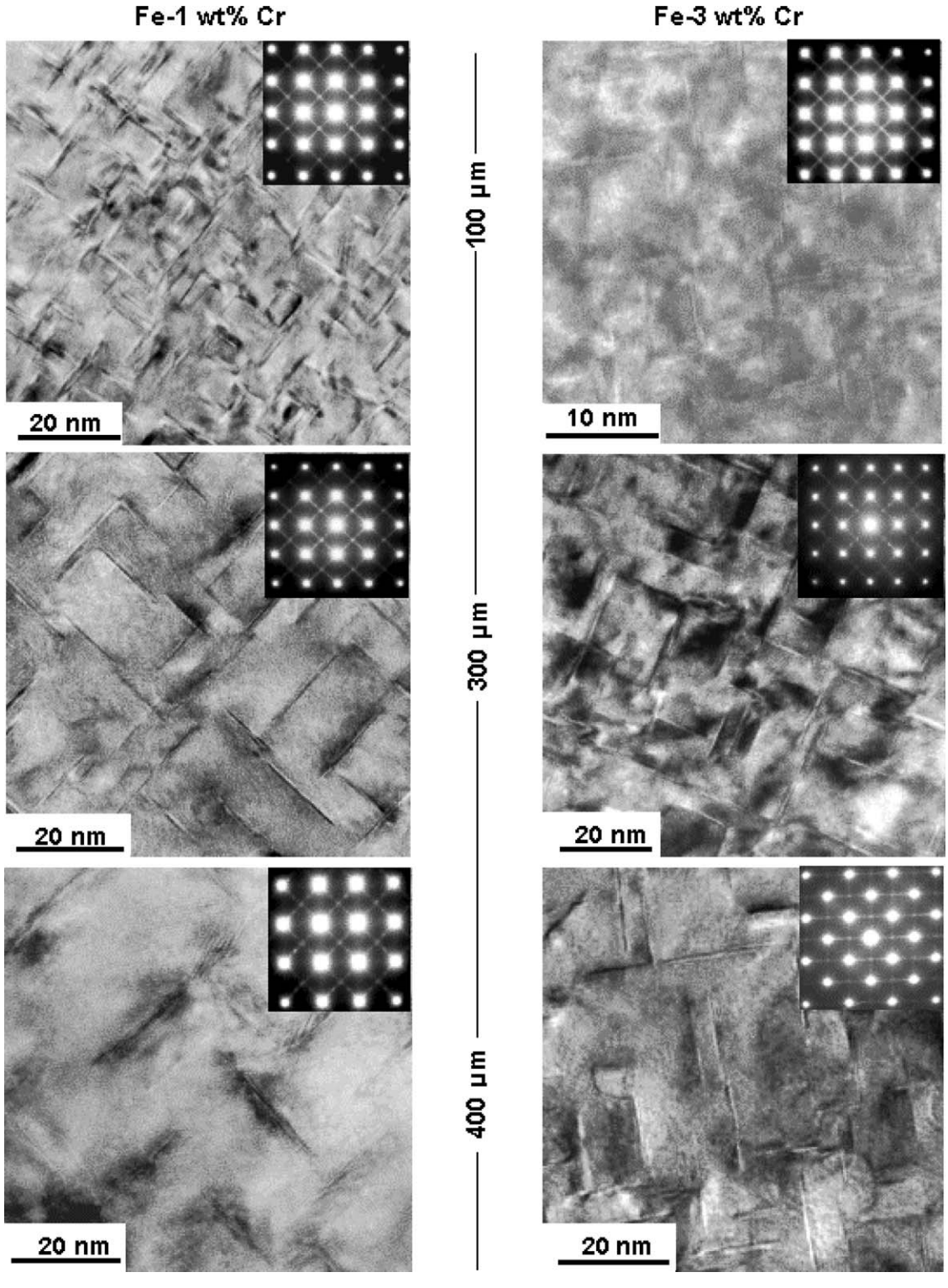

Figure 5 TEM micrographs and associated electron diffraction patterns showing the precipitation state evolution along the diffusion layer of 1 and 3 wt% Cr alloy nitrided 14 h at 823 K.

an identity of orientation between A_1 and B_1 zones which means that both zones belong to the same grain. The cell B_1 is thus formed by simple migration of the initial grain boundary A_1/C_1. The difference in color between the two areas is due simply to a permutation in the Euler angles play for the same orientation. In addition, it can be observed that grains A_1, C_1 are slightly disoriented ($\sim 8^\circ$) and have a common {110} plane (arrow).

3.2.2.2. Zone 2. As for zone 1, the mother grain, the discontinuous precipitation cell and the invaded grain are symbolized by A_2, B_2 and C_2 respectively. Firstly, one can notice from the corresponding poles figures (Fig. 8b) that A_2 and C_2 present exactly the same disorientation observed in zone 1 between A_1 and C_1 grains and they have also a {110} plane in common (arrow). These two characteristics could constitute initiating factors of the discontinuous precipitation reaction.

More interesting, poles figures also reveal that during growth the B_2 cell changes its orientation with respect to the mother grain and presents a singular crystallographic disposition:

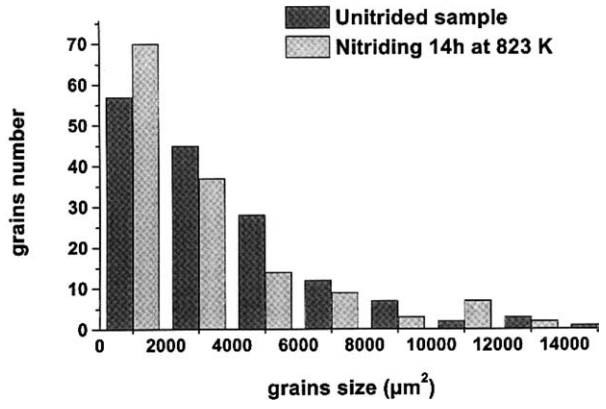

Figure 6 Histograms of the distribution of grain sizes in an unitrided and a nitrided Fe-3 wt% Cr alloys (14 h at 823 K).

(i) The B_2 cell is composed for two Σ3 twinned crystals B_{2a} and B_{2b} recognizable by a rotation of 60° around the [111] common axis;

(ii) (B_{2a}, B_{2b}) cells and C_2 grain have a ⟨110⟩-type common axis (double arrow) and are disorientated of an angle close to 38° around this axis which corresponds to a Σ9 twin boundary.

Σ3 and Σ9 boundaries are always located inside the discontinuous precipitation cells and at the border between cells and untransformed zones, respectively (Fig. 7c). These particular orientations are reproduced on all the discontinuous precipitation zone in the investigated region.

3.2.2.3. Zone 3. In this zone where the discontinuous precipitation growth is in an advanced stage, the crystallographic characteristics evoked in zone 2 are always respected (Fig. 8c). Indeed, by rotation of the {111} common poles of B_{3a} and B_{3b} (arrow) towards the center of the projection, one can realize that these two grains present a Σ3 twin boundary. Also, B_{3a}, B_{3b} and C_3 exhibit a common ⟨110⟩-type axis and a Σ9 twin boundary.

From these crystallographic aspects, it was deduced that the growth of a discontinuous precipitation cell is originates by the grain boundary migration. This mechanism is stopped after a short time leaving the place to a germination of new twinned grains (Σ3) separated by a Σ9 special boundaries from the old grain in which the precipitation cell is propagated. In fact, the conservation

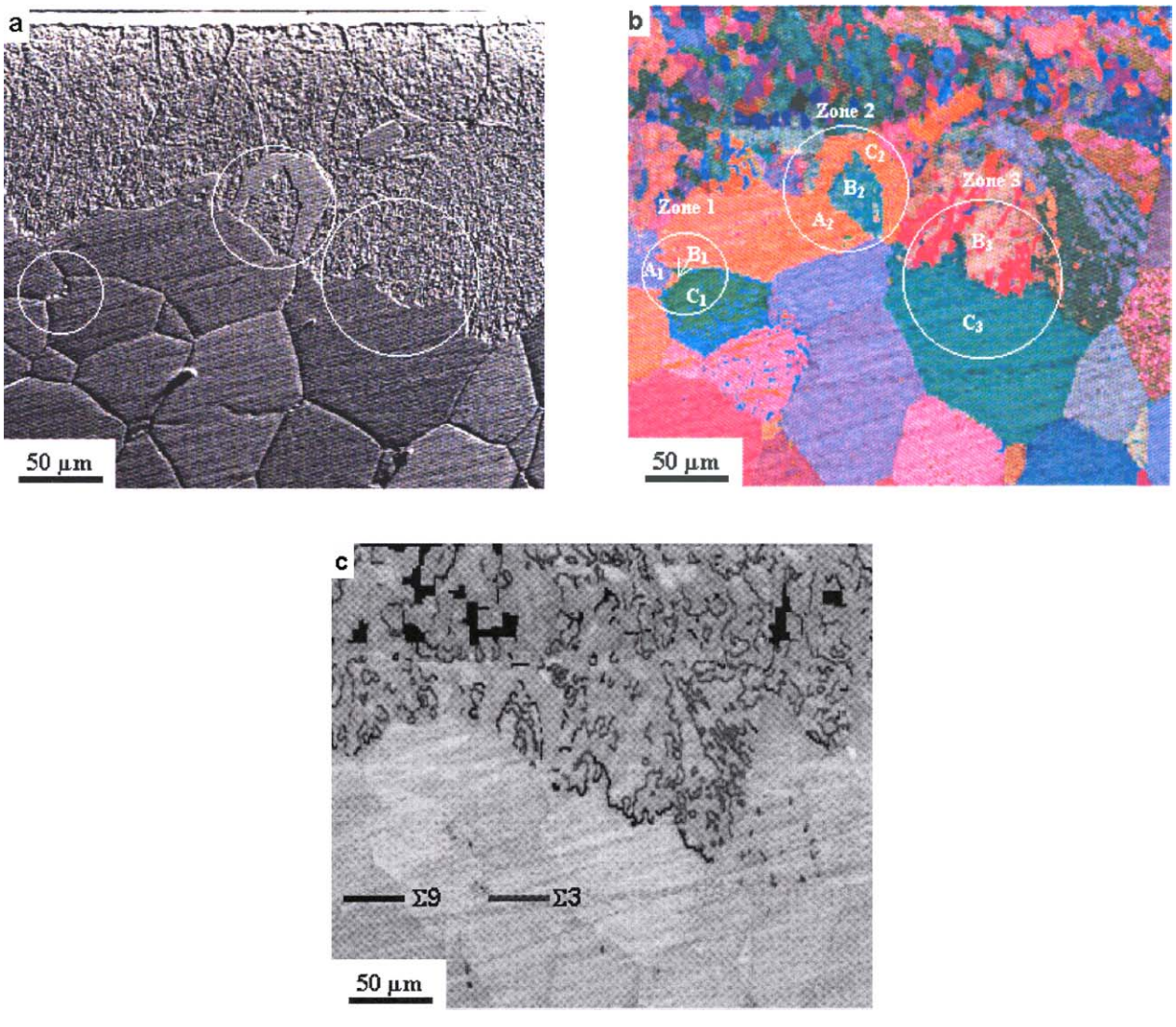

Figure 7 (a) Cross-sectional SEM micrograph of nitrided (14 h at 823 K) Fe-3 wt% Cr alloy showing CrN discontinuous precipitation at superficial zones. (b) EBSD map carried out on the same region. (c) EBSD map of Σ3 and Σ9 twin boundary location in discontinuous precipitation cells of Fig. (a).

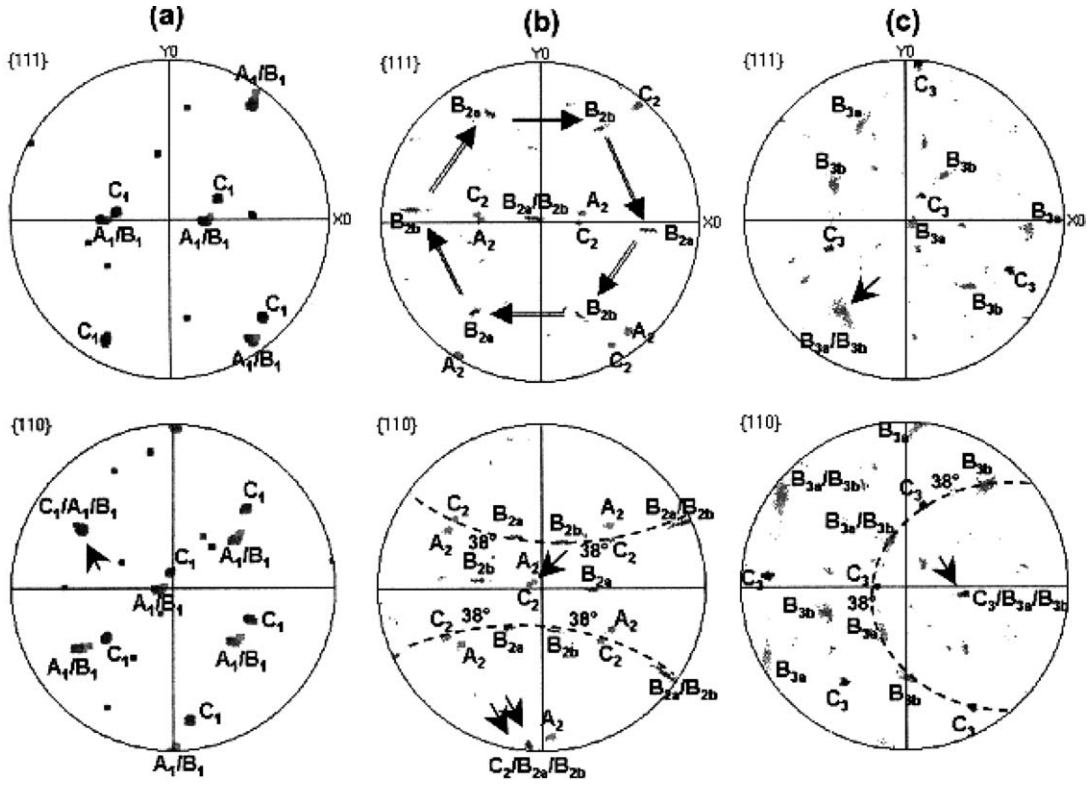

Figure 8 {111} and {110} poles figures corresponding to zone1, zone 2 and zone 3 in Fig. 7.

of the {110} close-packed plane in ferrite and the formation of Σ3 twin boundaries in transformed zones seem to be a constant of the reaction. These features clearly show the non-steady state character of the discontinuous precipitation development in nitrided Fe-Cr alloys compared to the steady state character in the "typical" discontinuous precipitation in binary substitutional systems such as Pb-Sn [16], Fe-Zn [17] and Mg-Al [18] alloys. In these last alloys, discontinuous precipitation is assimilated to the growth of parallel, plane and regularly spaced lamellas behind a moving grain boundary.

A qualitative explanation may be offered for the features of the present discontinuous precipitation. Firstly, discontinuous precipitation cells are initiated by grain boundary migration according to Tu and Turnbull mechanism [19]. Lamellas growth is controlled by volume and grain boundaries chromium diffusion at their tips. Thus, due to the high diffusion of chromium in iron, lamellas develop rapidly so much that they can go past the moving cell boundary and then grow in the neighbor grain adopting the Baker-Nutting (ORs). This will cause necessarily the stopping of the boundary migration because lamellas are no more in coherence relationship with the old grain. This process is synchronized with another. Indeed, the formation of each lamella causes a local volume expansion about 50% which constitutes a barrier to the discontinuous precipitation cell growth because of the plasticity which must be created around lamellas. The volume expansion will be sponged by iron self-diffusion and the created plasticity is eliminated by the recovery and recrystallization of the ferrite accompanied by the creation of Σ3 and Σ9

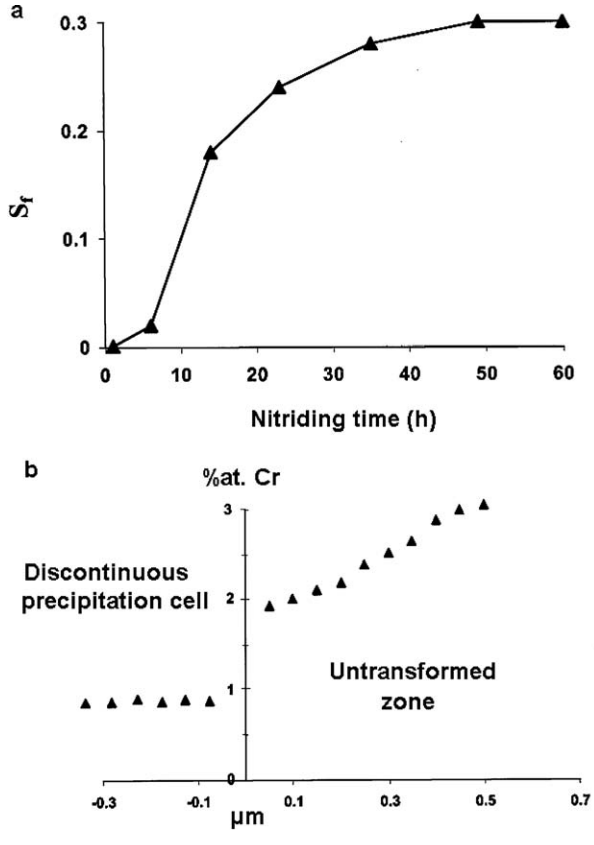

Figure 9 (a) Evolution of the surface fraction of the transformed zones (S_f) with nitriding time in the case of Fe-3 wt% Cr alloy. (b) Evolution of the atomic chromium concentration across discontinuous precipitation cell boundary in nitrided (14 h at 823 K) Fe-3 wt% Cr alloy.

*Such a value is obtained from the following considerations: the cell volume V_{CrN} of CrN (2Cr + 2N) is 0.07 nm^3 (a_{CrN} = 0.414 nm). We can consider in first approximation that each chromium atom in the iron matrix occupies the iron atomic volume V_{Fe} i.e $0.286^3/2$ nm^3 and that the nitrogen atomic volume inside matrix is negligible (interstitial position). The expansion due to the CrN growth is given by: $\frac{V_{CrN}/2-V_{Fe}}{V_{Fe}} = 0.52$.

twin boundaries in order to minimize the energy. So long as chromium and nitrogen continue to diffuse towards discontinuous precipitation cells, they continue to develop with nitriding time. Fig. 9a shows the evolution of the surface fraction of transformed zones (S_f) versus nitriding time.

Hence, we can see that lamellas grow rapidly during the first 20 h of nitriding but the driving force of the process decrease during prolonged nitriding and cells stop completely to develop after 50 h of nitriding although all the material is not entirely transformed.

Considering the rapid diffusion of interstitial nitrogen, it is reasonable to think that the kinetics of growth of the CrN discontinuous precipitation is controlled by the far slower grain boundary and volume diffusion of chromium. Furthermore, EDX analysis performed across a cell boundary revealed the existence of a poor chromium zone on about 500 nm ahead of the cell boundary (Fig. 9b), which indicates that chromium volume diffusion is predominant during prolonged nitriding. Therefore this can explain the reducing and then the stop of cell boundary migration even though the nitrogen supersaturation still remains in the untransformed matrix.

3.3. Effect of nitriding temperature

SEM micrographs obtained on Fe-1 wt% Cr samples nitrided at high temperature (873 K) reveal the development of a new phase in surface regions (Fig. 10a) identified by X-rays diffraction as an iron austenite (γ) phase (Fig. 10b). Nitriding temperature increasing also induces the growth, from ferrite grain boundaries, of needle-shape Fe_4N (γ') precipitates (Fig. 10c) which present the same morphology as those observed during aging of some nitrided ferrous materials [20]. The Fe-N phase diagram indicates that at 873 K, the $\alpha \rightarrow \gamma$ transformation occurs as soon as the nitrogen content exceeds the limit of solubility in ferrite which is about 0.1 wt% N.

Considering that the nitrogen is a good stabilizer of austenite, if the cooling is sufficiently fast, which is

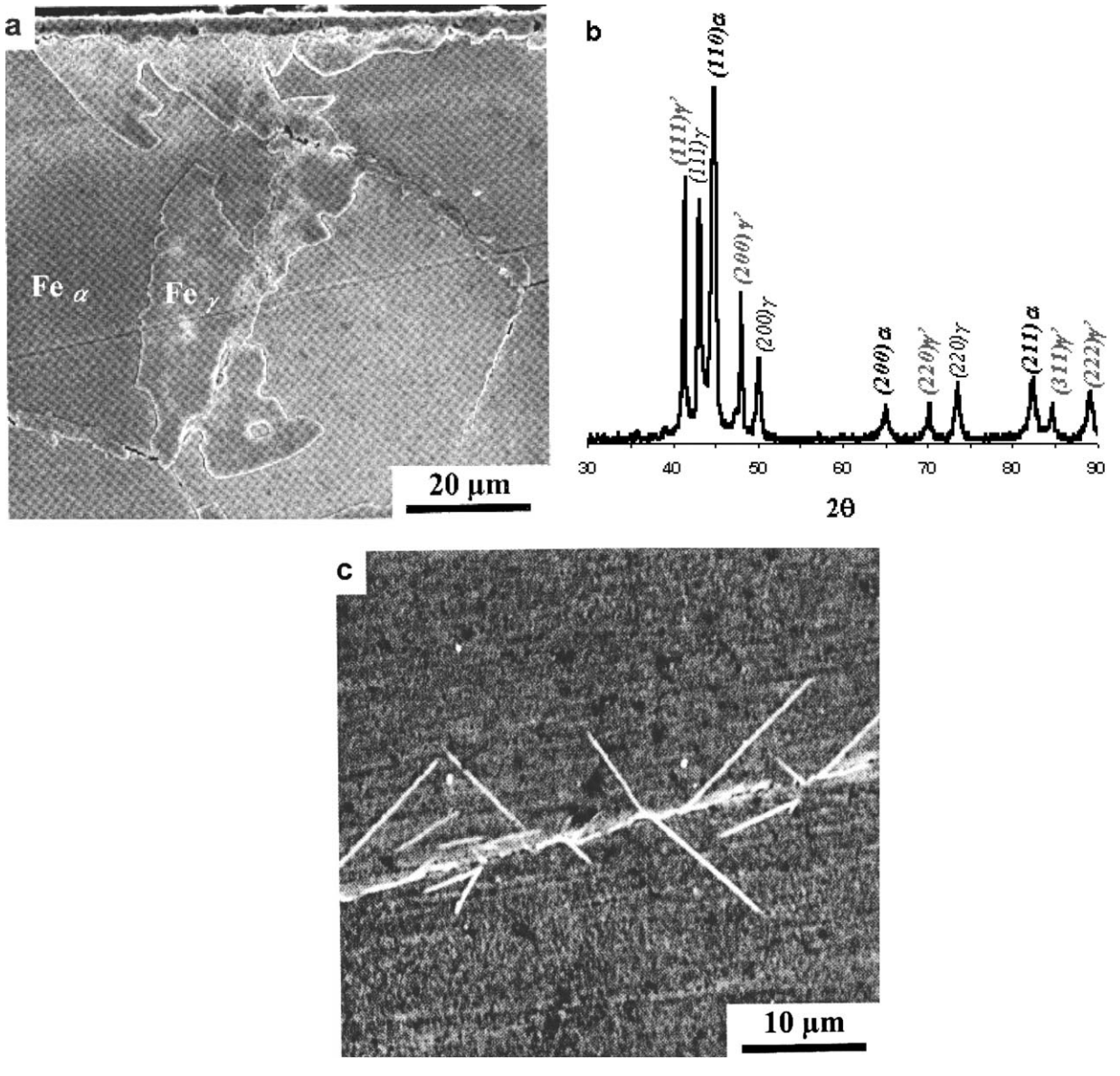

Figure 10 (a) Cross-sectional SEM micrograph of nitrided (14 h at 873 K) Fe-1 wt% Cr alloy. Rough zones close to the surface and grain boundaries were identified by X-ray diffraction (b) as being of retained austenite. For the same nitriding temperature, needle-shape Fe_4N precipitates are growing from grain boundaries (c).

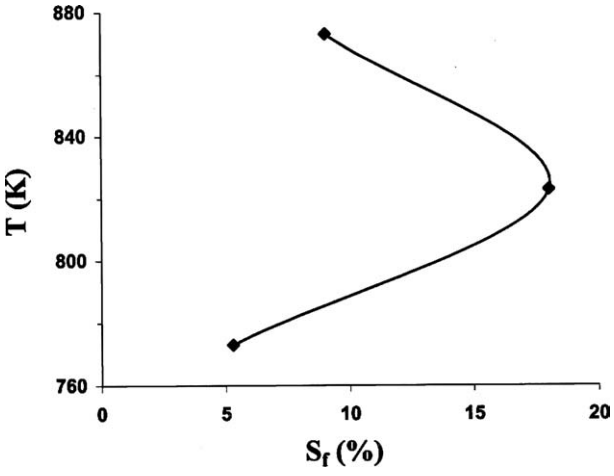

Figure 11 Evolution of the surface fraction of transformed zones (S_f) versus nitriding temperature (14 h nitriding time).

the case of the areas close to the surface, the reverse transformation is not complete leading to the coexistence of the two phases: ferrite and retained austenite. The nitrogen in solid solution in austenite would thus precipitate as CrN, which can explain the comparable microhardness of the two phases (the measured values are close to 650 Hv for both). Furthermore, the growth of Fe_4N precipitates occurs when nitrogen concentration reaches 5.8 wt% which can be achieved rapidly on grain boundaries in view of the high nitrogen diffusion through them.

On the other hand, relatively to the effect of nitriding temperature on discontinuous precipitation growth, Fig. 11 shows that, for 14 h nitriding time, surface fraction of transformed zones (S_f) varies like a C-curve with the maximum precipitation rate at about 823 K. This can be explained by the fact that at low temperature (773 K), due to a thermally activated process, the diffusion of nitrogen is relatively slow. Consequently, after a 14 h nitriding, only the areas located on the extreme surface are saturated in nitrogen and where CrN lamellas can grow. However, for high temperature nitriding (873 K), the nitrogen diffuses rapidly in iron matrix so that the supersaturation of the zones close to surface is decreased for the benefit of internal diffusion of nitrogen. The growth rate of discontinuous precipitation is thus considerably reduced.

4. Conclusion

Fe-Cr alloys (1 and 3 wt% Cr) investigated in this study, can serve as model systems for the more complex nitriding Cr alloy steels. For both Fe-Cr alloys, it has been shown that nitriding provides a high hardening of nitrided layer which was attributed to the fine and coherent precipitation of CrN. In addition, discontinuous precipitation of CrN starting from grain boundaries has been observed in the high chromium-containing alloy. Electron diffraction revealed that both nanometric and lamellar CrN have a cubic crystallographic structure (NaCl-type) exhibiting the Baker-Nutting (ORs) with respect to the iron matrix. HRTEM study of the microstructural characteristics evolution of the nitrided layer showed the increasing of the precipitates diameter with the nitriding depth associated to the reducing of their number per volume unit. Thus, this explain the profile of mechanical properties observed along the nitrided layer due to the diminution of pinning points for the moving dislocations.

Concerning the discontinuous precipitation of CrN, SEM images exploitation showed that lamellas start to grow in the early stage of nitriding in concurrence with the nanometric precipitation but they stop to grow before invading all the material while nitrogen supersaturation is still present in the untransformed matrix. Furthermore, EBSD investigations revealed that discontinuous precipitation growth is governed by specific crystallographic considerations. They consist in the apparition of $\Sigma 3$ twin-boundaries inside the discontinuous precipitation cells and $\Sigma 9$ boundaries in the border with the untransformed zones.

Concerning nitriding parameters, it was observed that nitriding temperature increasing results in the formation of retained austenite and the growth of Fe_4N nitrides from grain boundaries during high temperature (873 K) nitriding. Furthermore, discontinuous precipitation growth is significantly limited when nitriding temperature is strongly increased or decreased.

Finally, the obtained results should lead to a better understanding of nitrided steels microstructure and its role on the mechanical behavior. This study could also have effects on industrial steels nitriding conditions.

Acknowledgments

The authors would like to thank Ecole des Mines de Saint-Etienne for supplying the Fe-Cr alloys and SNR Roulements society (France) for the access to the BMI Furnace. Thanks are due to M. Pelloux for performing the nitriding treatments. We thank the Consortium Lyonnais de Microscopie Electronique (CLYME) for the access to the Jeol 2010F and Jeol 200CX microscopes, and the Consortium des Moyens Technologiques Communs (INPG- Grenoble) for access to the CAMEBAX SX electron microprobe.

References

1. H. ELGHAZAL, G. LORMAND, A. HAMEL, D. GIRODIN and A. VINCENT, *Mater. Sci. Eng.* A **303** (2001) 110.
2. C. JACQ, G. LORMAND, D. NÉLIAS, D. GIRODIN and A. VINCENT, *ibid.* **342** (2003) 311.
3. L. BARRALIER, PhD thesis, ENSAM de Aix en Provence, 1992.
4. D. H. JACK and K. H. JACK, *Mater. Sci. Eng.* **1** (1973) 1.
5. B. MORTIMER, P. GRIEVESON and K. H. JACK, *Scan. J. Metall.* **1** (1972) 203.
6. H. C. F. HEKKER, P. M. ROZENDAAL and E. J. MITTEMEIJER, *J. Mater. Sci.* **20** (1985) 718.
7. P. C. VAN WIGGEN, H. C. F. ROZENDAAL and E. J. MITTEMEIJER, *ibid.* **20** (1985) 4561.
8. D. B. WILLIAMS and E. P. BUTLER, *Inter. Met. Rev.* **3** (1983) 153.
9. M. KIKUCHI, M. KAJIHARA and S. CHOI, *Mater. Sci. Eng.* A **146** (1991) 131.
10. N. C. SANTHI SRINVAS and V. V. KUTUMBARAO, *Scripta Mater.* **37** (1997) 285.
11. Y. USTINOVSHIKOV, A. RUTS, O. BANNYKH and V. BLINOV, *Acta. Mater.* **44** (1995) 1119.

12. Y. USTINOVSHIKOV, A. RUTS, O. BANNYKH, V. BLINOV and M. KOSTINA, *Mater. Sci. Eng.* A **262** (1999) 82.
13. F. VANDERSCHAEVE, R. TAILLARD and J. J. FOCT, *Mater. Sci.* **30** (1995) 6035.
14. M. SENNOUR, PhD thesis, INSA de Lyon (2002) p. 156.
15. B. J. LIGHTFOOT and D.H. JACK, in Proceedings of the Conference on Heat Treatment, 1973 (The Metals Society, London, 1975) p. 59.
16. K. N. TU and D. TURNBULL, *Acta. Metall.* **15** (1967) 369.
17. D. TURNBULL and H. N. TREAFTIS, *Trans AIME.* **212** (1958) 33.
18. S. K. BUDUROV, G. RUSSEV, A. ZLATEV and R. PETROV, *Z. Metallkde.* **70** (1973) 372.
19. D. B. WILLIAMS and E. P. BUTLER, *Int. Met. Rev.* **3** (1981) 153.
20. G. HINOJOSA, J. OSEGUERA and P. S. SCHABES-RETCHKIMAN, *Thin Solid Films* **349** (1999) 171.

Received 10 July 2003
and accepted 5 March 2004